American Mineralogist, Volume 81, pages 902–912, 1996

Trace element zoning and incipient metamictization in a lunar zircon: Application of three microprobe techniques

BRIGITTE WOPENKA,[1] BRADLEY L. JOLLIFF,[2] ERNST ZINNER,[2] AND DANIEL T. KREMSER[1]

[1]Department of Earth and Planetary Sciences, Washington University, St. Louis, Missouri 63130-4899, U.S.A.
[2]Department of Earth and Planetary Sciences and McDonnell Center for the Space Sciences, Washington University, St. Louis, Missouri 63130-4899, U.S.A.

ABSTRACT

We have determined major (Si, Zr, Hf), minor (Al, Y, Fe, P), and trace element (Ca, Sc, Ti, Ba, REE, Th, U) concentrations and Raman spectra of a zoned, 200 μm zircon grain in lunar sample 14161,7069, a quartz monzodiorite breccia collected at the Apollo 14 site. Analyses were obtained on a thin section in situ with an ion microprobe, an electron microprobe, and a laser Raman microprobe. The zircon grain is optically zoned in birefringence, a reflection of variable (incomplete) metamictization resulting from zonation in U and Th concentrations. Variations in the concentrations of U and Th correlate strongly with those of other high-field-strength trace elements and with changes in Raman spectral parameters. Concentrations of U and Th range from 21 to 55 ppm and 6 to 31 ppm, respectively, and correlate with lower Raman peak intensities, wider Raman peaks, and shifted Si-O peak positions. Concentrations of heavy rare earth elements range over a factor of three to four and correlate with intensities of fluorescence peaks. Correlated variations in trace element concentrations reflect the original magmatic differentiation of the parental melt ~4 b.y. ago. Degradation of the zircon structure, as reflected by the observed Raman spectral parameters, has occurred in this sample over a range of α-decay event dose from $\sim 5.2 \times 10^{14}$ to 1.4×10^{15} decay events per milligram of zircon, as calculated from the U and Th concentrations. This dose is well below the $\sim 10^{16}$ events per milligram cumulative dose that causes complete metamictization and indicates that laser Raman microprobe spectroscopy is an analytical technique that is very sensitive to the radiation-induced damage in zircon.

INTRODUCTION

The metamictization of zircon has been the subject of extensive research (e.g., Holland and Gottfried 1955; Pidgeon et al. 1966; Chakoumakos et al. 1987; Murakami et al. 1991; Woodhead et al. 1991; Ellsworth et al. 1994; Weber et al. 1994). Understanding how the zircon structure responds to radiation damage is important for both the storage of high-level radioactive waste (e.g., Ewing et al. 1995) and the use of U-Th-Pb isotopic systematics in zircon. In the latter case, the fracturing due to volume expansion that accompanies metamictization may lead to diffusive loss or heterogeneous redistribution of radiogenic Pb (e.g., Compston et al. 1989; Meyer et al. 1989a), as well as make zircon more susceptible to chemical alteration during metamorphism or chemical weathering (Tilton 1960; Silver and Deutsch 1963; Williams et al. 1984; Black et al. 1991; Pidgeon 1992; McLaren et al. 1994). Numerous studies have attempted to determine the approximate α-decay event dose at which zircon begins the crystalline-to-amorphous transition (e.g., Chakoumakos et al. 1987; Woodhead et al. 1991; Murakami et al. 1991; Ellsworth et al. 1994). There is also evidence that the metamictized structure of zircon recovers or recrystallizes somewhat over geologic time (Weber et al. 1994).

The metamictization of zircon can be characterized by Raman spectroscopy (Jolliff et al. 1995; Nasdala et al. 1995). The present study is part of a broader effort to investigate the Raman and fluorescence spectra of zircon for which age and U and Th concentrations are known and to correlate these spectra with their major and trace element chemical compositions. We report Raman spectral characteristics of a lunar zircon grain that was selected in part because it is chemically zoned in an apparently simple and understandable manner, consistent with its formation in a mineralogically and chemically simple system, in comparison with terrestrial counterparts. Furthermore, the lunar zircon formed under anhydrous conditions and has not been exposed to multiple episodes of thermal metamorphism or chemical weathering, as is commonly the case for terrestrial zircon that is subjected to crustal recycling.

0003–004X/96/0708–0902$05.00

Structure, chemistry, and optical characteristics of zircon

Zircon occurs as a widespread accessory mineral in almost all types of terrestrial rocks, but it also occurs in meteorites and lunar rocks. It is one of the earliest accessory minerals to crystallize in a magma and continues to precipitate over long periods of time and ranges of temperature. Individual crystals can develop extensive chemical zonation, which reflects the changing chemical composition of residual magma (Hinton and Upton 1991).

As summarized by Speer (1982), the chemical composition of zircon is complex, and besides Hf, which is always present (concentrations up to 7 wt%), more than 50 other elements have been found in zircon. The most important ions substituting for $^{[8]}Zr^{4+}$ are Hf^{4+}, U^{4+}, Th^{4+}, Y^{3+}, and the REE^{3+}. Only P^{5+} and sometimes Nb^{5+} and Al^{3+} can replace Si^{4+} in its tetrahedral site. A close correlation between the concentrations of atoms of P and REE (including Y) in many zircon crystals suggests that most of the REEs are present in the form of phosphate molecules (i.e., $REEPO_4$) as in xenotime (YPO_4).

The incorporation of various elements substituting for Zr^{4+} changes the physical characteristics of the mineral and results in optical zonation, metamictization, and fluorescence. Transmission electron microscopy on zoned single crystals of zircon reveals that some of the zones are perfectly crystalline, whereas other zones show some structural damage or are even amorphous (Murakami et al. 1991). Metamictization in zircon results from α-decay events in the natural radioactive decay of ^{238}U, ^{235}U, and ^{232}Th and their daughter products. Specifically, the high-energy α particle produces hundreds of atomic displacements with a range of ~ 10 μm, and the energetic recoil nucleus, with a range of ~ 20 nm, produces localized damage with about 1000 atomic displacements (Weber et al. 1994). Zircon may contain substantial concentrations of U and Th and may therefore be exposed to doses as high as 10^{15}–10^{16} α-decay events per milligram of zircon over its geologic life time. The physical changes in zircon that result from radiation damage include an increase in unit-cell dimensions and decreases in density and hardness (Holland and Gottfried 1955; Speer 1982). The different interference colors frequently observed in thin sections of zircon are known to be due to differing levels of α-decay damage. Increasing radiation damage decreases birefringence until the fully metamict crystal is optically isotropic (Sahama 1981). The totally metamict state is a structure that appears to be amorphous when analyzed by X-ray and electron diffraction techniques (e.g., Yada et al. 1981).

Sample

We report here the analytical results obtained on a single zoned zircon grain in a thin section of a 23 mg lithic fragment, lunar sample 14161,7069, from an Apollo 14 soil. This sample is a partially recrystallized impact breccia of quartz-monzodioritic (QMD) bulk composition and mineralogy, including regions of potassium feldspar–bearing granophyre (Jolliff et al. 1991; Jolliff 1991). The unusually high incompatible trace element concentrations (ITE $\approx 2\times$ average high-K KREEP; Warren 1989), low siderophile-element concentrations, and uniform major mineral compositions indicate that this breccia is monomict (Jolliff 1991; Warren 1993). The original 23 mg sample comprised ~ 30 vol% pyroxene (average $En_{24}Fs_{68}Wo_8$ and $En_{20}Fs_{52}Wo_{28}$), ~ 30% plagioclase (An_{78-61}), 23% quartz plus silica–potassium feldspar granophyre, 11% barian potassium feldspar, 3.7% phosphates (whitlockite, apatite), 2.4% ilmenite, approximately 0.6% zircon, and a trace of fayalite (Jolliff 1991). Baddeleyite (ZrO_2), zirconolite [$(Fe,Ca,REE)(Zr,Ti,REE)_3O_7$; Wark et al. 1973], and yttrobetafite [$(Ca,Fe,Y,REE,U,Th)_2(Ti,Nb)_2O_7$; Meyer and Yang 1988], which have been found in other evolved lunar rocks (e.g., Smith and Steele 1976), were not found in the thin section of 14161,7069; however, the high bulk Th concentration of the sample (44 ppm; Jolliff 1991) suggests the presence in the rock sample of a Th-rich phase. Sample 14161,7069 was derived from a rock that was brecciated by a meteorite impact at ~ 4 Ga. We suspect the zircon to be older, perhaps as old as 4.1–4.35 Ga, by analogy to other samples of lunar granite and quartz monzodiorite (Compston et al. 1984; Shih et al. 1985, 1993; Meyer et al. 1989b, 1991).

The zircon grain we selected is a clast (about 200 × 80 μm), a fragment of an originally larger crystal, and was analyzed in a polished thin section of ~ 10–15 μm thickness. The mounting medium was Araldite, which does not show any laser-induced fluorescence and thus does not interfere with a successful interpretation of the Raman spectra obtained from the sample. The zircon grain is fractured, but it is free of mineral inclusions (Figs. 1a and 1b). Fractures extend into the surrounding matrix but appear to be related to the sample's impact history, not to radiation damage in the zircon. In cross-polarized light, zoning appears as a change in interference colors across the zircon grain, and in the backscattered electron image (Fig. 1b), the bright area on the right side of the grain indicates a high concentration of elements heavier than Zr, such as U, Th, and REE. From the optical appearance in cross-polarized light, and from the backscattered electron image, we inferred this grain to be zoned in chemical composition.

Analytical characterization

The chemical composition and some vibrational spectroscopic characteristics were determined with an ion microprobe, an electron microprobe, and a Raman microprobe. All three microprobe techniques were applied to the same five points labeled A, B, C, D, and E (Fig. 1c) to characterize chemical and structural variations normal to the optical zoning of the grain. The individual measurement points can be seen easily in the backscattered electron image (Fig. 1b) that was obtained after the sam-

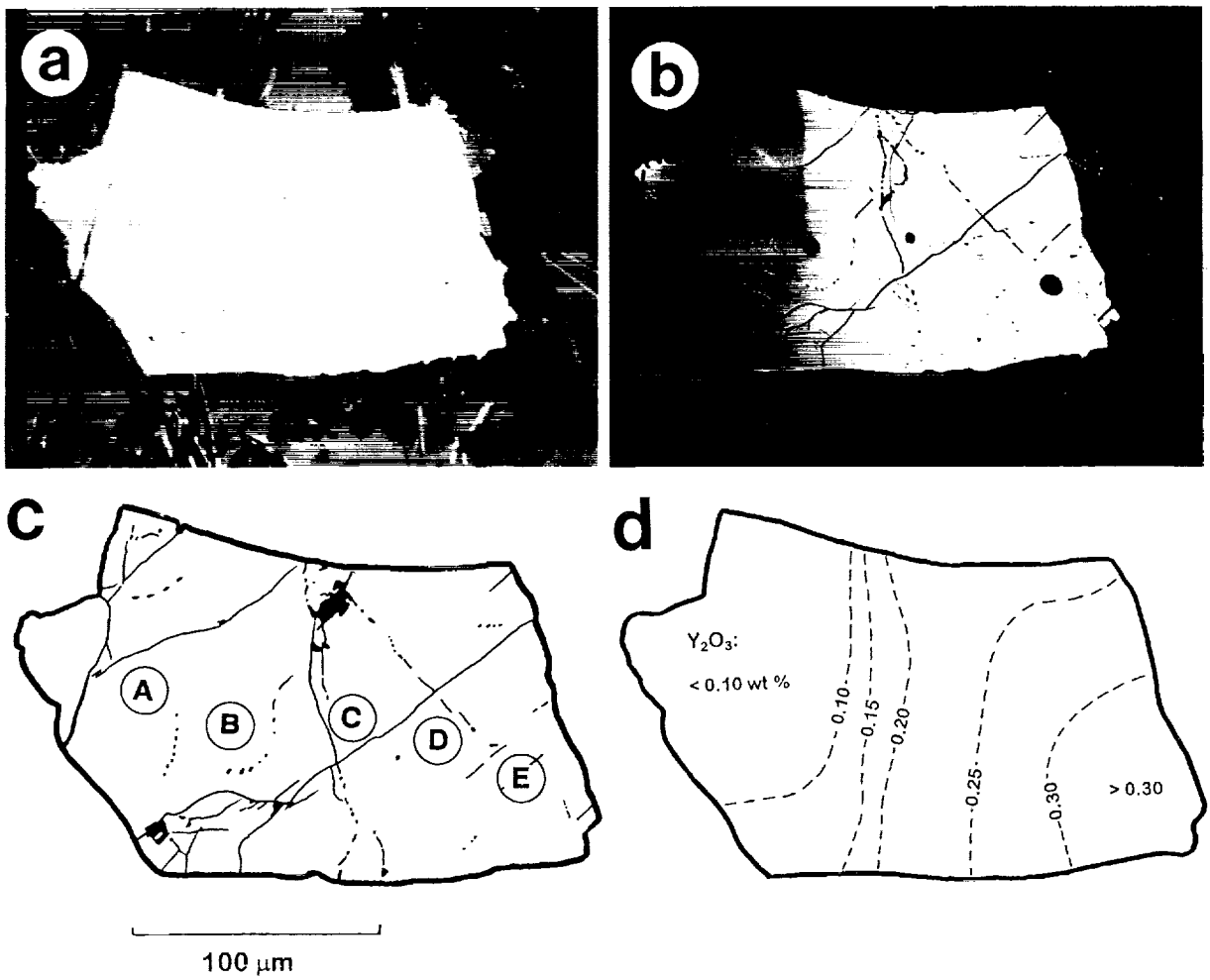

FIGURE 1. Zircon grain (approximately 200 × 80 μm) in lunar sample 14161,7069. (**a**) Backscattered electron image (BEI) shows the zircon grain in a matrix of plagioclase (dark gray), pyroxene (lighter gray, somewhat poikilitic), and ilmenite (bladed). Other minerals include potassium feldspar (lighter patches in plagioclase) and phosphates (thin blades, not as bright as ilmenite). (**b**) BEI adjusted for maximum contrast across zircon grain. Chemical zoning appears as a change in brightness and as a change in interference colors in transmitted, cross-polarized light (not shown). Darker region on left has lowest concentrations of heavy trace elements. The ion microprobe analysis spots are visible as nearly circular marks (see c). Note that there is no zircon overgrowth on the outer edge of the grain, and that the chemical zoning truncates at the grain edge. (**c**) Sketch of same sample. Circled letters mark locations of ion microprobe, electron microprobe, and Raman microprobe analyses referred to in the text. (**d**) Sketch showing contours of Y_2O_3 concentrations on the basis of gridded (20 μm spacings), electron microprobe wavelength-dispersive analyses of yttrium and backscattered electron imaging.

ple was subjected to ion microprobe analysis. Raman microprobe analysis was performed before ion microprobe analysis to preclude any change in crystalline structure that possibly might be caused by the ion sputtering process. No special sample preparation is needed for Raman analysis, whereas the other two techniques require a carbon coat on the thin section.

Elemental composition

Major and minor element concentrations were obtained by wavelength-dispersive analysis using a JEOL 733 electron microprobe equipped with automation of Advanced Microbeam, Inc. For these electron microprobe analyses, we used an accelerating voltage of 15 kV, a beam current of 30 nA, and a beam diameter of 1–10 μm. The primary standards were as follows (C.M. Taylor Corporation, Stanford, California): zircon for Zr and Si, synthetic $(Zr,Hf)O_2$ for Hf, hematite for Fe, YAG garnet for Al and Y, and synthetic $YbPO_4$ (Jarosevich and Boatner 1991) for P and Yb. X-ray matrix corrections were based on a modified Armstrong (1988) CITZAF routine. In addition to spot analyses along a traverse matching those made by the ion and Raman microprobes, quantitative analyses in a grid pattern across the grain at ~20 μm spacing were obtained (see Fig. 1d).

Trace element analyses were made in situ with a mod-

ified CAMECA IMS 3F ion microprobe. The technique of trace element measurements by secondary ion mass spectrometry (SIMS) in the energy-filtering mode was described by Zinner and Crozaz (1986). The analysis of certain trace elements in zircon presents special problems that are usually not encountered during the analysis of these elements in other silicate minerals. For instance, the determination of Sc concentrations in zircon is even more complicated than in other silicates because, in addition to $^{29}Si^{16}O$, $^{90}Zr^{2+}$ interferes with $^{45}Sc^{+}$ at mass 45 (Sc has only one stable isotope). To determine the Sc^{+} signal, the ion signals at the masses 40, 42, 44, 45, 46, 48, and 49 were deconvolved into contributions from Ca^{+}, MgO^{+}, SiO^{+}, Sc^{+}, Zr^{2+}, and Ti^{+} (mass 47 could not be used because of the presence of a PO^{+} signal). Another problem in the analysis of trace elements in zircon is the interference of $ZrSiO^{+}$ ions with the signals from La ($^{94}Zr^{29}Si^{16}O$ at mass 139), Ce ($^{96}Zr^{28}Si^{16}O$ and $^{94}Zr^{30}Si^{16}O$ at mass 140 and $^{96}Zr^{30}Si^{16}O$ at mass 142), Pr ($^{96}Zr^{29}Si^{16}O$ at mass 141), and Nd ($^{96}Zr^{30}Si^{16}O$ at mass 142). These interferences are usually negligible, but in zircon, which typically has low concentrations of the light REEs (Hinton and Upton 1991), they can become significant. These interferences were corrected by obtaining ion signals at the masses 134, 138, 139, 140, 141, and 142 and deconvolving them into contributions from $ZrSiO^{+}$, Ba^{+}, La^{+}, Ce^{+}, Pr^{+}, and Nd^{+}. Hydride contributions from contamination by H-bearing species in the sample chamber usually do not need correction, except for the determination of P, which has only one stable isotope, ^{31}P. The SiH^{+} signal was determined by deconvolution of the signals at masses 29 and 30 into contributions from Si^{+} and SiH^{+}, and the $^{30}SiH^{+}$ signal was subtracted from the ion signal at mass 31 to obtain the P^{+} signal. The ion signal at mass 93, where Nb has its only stable isotope, is dominated by $^{92}ZrH^{+}$. However, by estimating the ZrH^{+} signal from $^{94}ZrH^{+}$ at mass 95, we can set an upper limit of ~5 ppm on the Nb concentration.

In the absence of a suitable zircon standard with known trace element concentrations, sensitivity factors were determined from other silicate standards (Crozaz and Zinner 1986; Ireland et al. 1991) for all elements except Th and U. The sensitivity factors for the latter two elements were determined from a suite of terrestrial zircon samples with known Th and U concentrations. Both the atomic and the monoxide ion signals were recorded for Th and U, and, although they both show comparable intensities, only the atomic signals of $^{232}Th^{+}$ and $^{238}U^{+}$ were used. The positive-ion yields of Th and U relative to Si were 1.28 and 1.51, respectively. The use of the sensitivity factors determined in silicates other than zircon might result in systematic errors for absolute element concentrations (although our past experiences indicate that these errors are probably small), but relative differences in concentrations at different grain locations, especially of the magnitude observed in the lunar zircon of this study, should be accurately reflected by the data.

The electron and ion microprobe analyses confirmed chemical zoning, as suggested by variations in birefringence and from the backscattered electron image. Table 1 lists the measured major element (calculated as oxides) and trace element concentrations in all five sampling points. There is no significant difference in the concentrations of the major elements Zr, Si, and Hf across the grain. In contrast, the concentrations of heavy trace elements vary by factors ranging from three to five across the traverse of the grain. The concentrations of all trace elements are low on the left side of the grain (point A) and are significantly higher on the right side of the grain (point E; see Figs. 1c and 1d).

Vibrational spectroscopic characterization

The Raman spectroscopic and laser-induced fluorescence measurements were made in situ with a Jobin Yvon S-3000 triple-monochromator laser Raman microprobe with multichannel detection. The instrument consists of a 320 mm double-monochromator with two gratings of 600 grooves/mm in subtractive mode and a 1 m third stage with interchangeable gratings (600 grooves/mm were used). We used either the 487.999 or 514.532 nm line of an 1 W argon ion laser (Lexel 85–1). The theoretical diffraction-limited focal-spot diameter at the sample surface is about 1 μm for a high-numerical-aperture objective such as the Olympus 80× ultra-long-working-distance objective (N.A. = 0.75). The laser power at the sample surface is 10 mW, which is typically nondestructive to samples of geologic interest. However, in cases of trace element–rich and metamict zircon, an unusual sensitivity to the exciting laser was noted that can result in the melting of the mounting medium beneath the section, even though the zircon itself remains unaffected. The 180° backscattered light was detected with a 1 in., 1024-element, proximity-focused, intensified, optical diode-array detector. The spectra are reported with a spectral resolution of about 7 cm^{-1} and a wavenumber accuracy of about ± 1 cm^{-1}.

Conventional Raman spectroscopy is concerned with the Stokes Raman shift, which is the portion of the inelastically scattered light that is increased in wavelength. A Raman spectrum is a plot of the intensity of the inelastically scattered radiation (measured in photons per second) as a function of the Stokes Raman shift. To make the Raman peak positions independent of the wavelength of excitation, the position of a Raman peak is expressed in units of relative wavenumbers or delta wavenumbers (Δcm^{-1}), which is the difference in frequency between the exciting laser radiation and the Raman-scattered radiation. Depending on the specific molecular bond excited, Raman shifts occur between 100 Δcm^{-1} (corresponding to 517 nm for 514 nm excitation) and 4100 Δcm^{-1} (corresponding to 652 nm for 514 nm excitation).

The laser Raman microprobe also can be used as a photoluminescence microprobe in which laser-induced fluorescence-emission spectra can be obtained with both a high spatial resolution of 2 μm and a spectroscopic resolution as good as 1 cm^{-1} or 0.03 nm. This allows nar-

TABLE 1. Composition of zircon in lunar sample 14161,7069

	A	B	C	D	E	EMP Avg*
			Oxides (wt%) by EMP, except as noted			
SiO_2	32.5 ± 0.18**	32.8 ± 0.18	32.8 ± 0.18	32.6 ± 0.18	32.7 ± 0.18	32.4(0.54)
ZrO_2	66.2 ± 0.54	65.1 ± 0.54	66.5 ± 0.55	65.8 ± 0.55	66.3 ± 0.54	65.9(1.18)
HfO_2	1.28 ± 0.08	1.37 ± 0.08	1.22 ± 0.08	1.28 ± 0.08	1.24 ± 0.08	1.18(0.06)
Al_2O_3	<0.05	<0.05	<0.05	<0.05	<0.05	0.02(0.05)
Y_2O_3	0.07 ± 0.03	0.16 ± 0.03	0.23 ± 0.03	0.28 ± 0.04	0.34 ± 0.05	0.19(0.09)
FeO	0.10 ± 0.01	0.02 ± 0.01	0.02 ± 0.01	0.05 ± 0.01	0.06 ± 0.01	0.10(0.09)
P_2O_5	0.05 ± 0.01	0.09 ± 0.01	0.13 ± 0.02	0.16 ± 0.02	0.18 ± 0.02	0.11(0.05)
Ln_2O_3†	0.05	0.08	0.13	0.16	0.16	0.12(0.08)
Sum	100.3	99.6	101.1	100.4	101.0	100.0
			Trace elements (parts per million) by SIMS			
P	227 ± 13	380 ± 13	566 ± 13	715 ± 14	766 ± 16	
Ca	38 ± 8	24 ± 2	63 ± 10	125 ± 5	70 ± 5	
Sc	49 ± 10	58 ± 12	59 ± 12	69 ± 14	72 ± 14	
Ti	59 ± 2	66 ± 2	80 ± 4	79 ± 3	161 ± 5	
Y	776 ± 7	1250 ± 9	2136 ± 10	2519 ± 14	2660 ± 15	
Ba	1.8 ± 0.4	1.1 ± 0.3	1.8 ± 0.5	2.7 ± 0.5	7.5 ± 1.0	
La	0.2 ± 0.05	0.1 ± 0.05	0.4 ± 0.1	2.4 ± 0.2	0.4 ± 0.1	
Ce	0.7 ± 0.1	0.5 ± 0.1	1.7 ± 0.2	6.7 ± 0.6	2.3 ± 0.3	
Pr	0.1 ± 0.05	0.1 ± 0.05	0.3 ± 0.1	1.1 ± 0.1	0.6 ± 0.1	
Nd	0.9 ± 0.1	1.5 ± 0.1	4.9 ± 0.3	7.6 ± 0.5	7.3 ± 0.6	
Sm	2.0 ± 0.2	3.3 ± 0.3	8.3 ± 0.5	11 ± 1	10 ± 1	
Eu	0.05 ± 0.02	0.03 ± 0.02	0.12 ± 0.06	0.03 ± 0.06	0.03 ± 0.10	
Gd	14 ± 1	23 ± 1	49 ± 1	72 ± 1	68 ± 2	
Tb	3.3 ± 0.3	5.9 ± 0.4	11 ± 1	17 ± 1	14 ± 1	
Dy	58 ± 1	90 ± 2	167 ± 3	222 ± 3	213 ± 4	
Ho	22 ± 1	35 ± 1	60 ± 1	77 ± 1	78 ± 2	
Er	113 ± 2	171 ± 2	291 ± 4	344 ± 4	358 ± 4	
Tm	23 ± 1	36 ± 1	55 ± 1	68 ± 1	71 ± 2	
Yb	197 ± 3	286 ± 5	438 ± 6	499 ± 5	540 ± 9	
Lu	30 ± 2	8 ± 4	14 ± 5	76 ± 3	15 ± 7	
Th	6 ± 0.5	11 ± 0.5	21 ± 1	29 ± 2	31 ± 2	
U	21 ± 1	31 ± 2	44 ± 2	51 ± 2	55 ± 2	
			Calculated Th and U concentrations (ppm) at 4.0 Ga			
Th	7.3	13	26	35	38	
U	46	69	98	113	122	
			Calculated cumulative α-decay events per milligram of zircon			
Σ α-decay events	0.52×10^{15}	0.77×10^{15}	1.1×10^{15}	1.3×10^{15}	1.4×10^{15}	

* Average of 58 electron microprobe analyses (not normalized). Parentheses contain one standard deviation values; these values reflect compositional zoning, so they exceed analytical uncertainty.

** Analytical uncertainty for data points A–E (± values) represents one standard deviation on the basis of counting statistics.

† Ln_2O_3, lanthanides, determined by SIMS; see individual elements for analytical uncertainty. Ln_2O_3 value was summed for all trivalent lanthanides and extrapolated for those not measured.

row-line fluorescence spectra to be recorded on a micrometer scale in zoned minerals. The mechanical configuration of the high-resolution monochromator in combination with an argon ion laser as excitation source makes it possible to monitor the fluorescence-emission spectra between the wavelength of excitation (488 or 514 nm) and 850 nm. In general, laser-induced fluorescence is an undesired phenomenon in Raman spectroscopy because it typically interferes with and overwhelms the desired Raman spectroscopic information to the extent that the Raman spectrum cannot be interpreted. However, there are certain transitions of trace element ions, e.g., certain trivalent REE ions, that do not overlap or interfere with the Raman peaks, and whose fluorescence emission spectrum can be monitored in addition to the Raman spectrum.

Six of the observed peaks in the Raman spectrum of pure zircon (Fig. 2a) were theoretically assigned by Dawson et al. (1971) according to a full crystal-field analysis of the silicate tetrahedra in a crystalline structure with a D_{4h} point-group symmetry (Table 2). The four highest frequency modes are internal stretching and bending vibrations of the $(SiO_4)^{4-}$ tetrahedra; whereas, the modes at 224 and 201 Δcm^{-1} are lattice modes. The intensity of the bands with the E_g symmetry (see Table 2) depends on the orientation of the zircon crystal with respect to the polarization plane of the exciting laser light.

The optical spectrum of zircon obtained with a laser Raman microprobe consists not only of the Raman scattering from allowed vibrational modes but also of the structure- and site-specific fluorescence of trivalent REE ions (REE^{3+}). Many terrestrial zircon samples yield Raman spectra that are substantially different from the one predicted from the crystalline structure and obtained for pure $ZrSiO_4$ (Jolliff et al. 1995; Nasdala et al. 1995). The Raman peaks are frequently shifted substantially downward or upward in position, the peaks are wider, and additional peaks (which are caused by laser-induced flu-

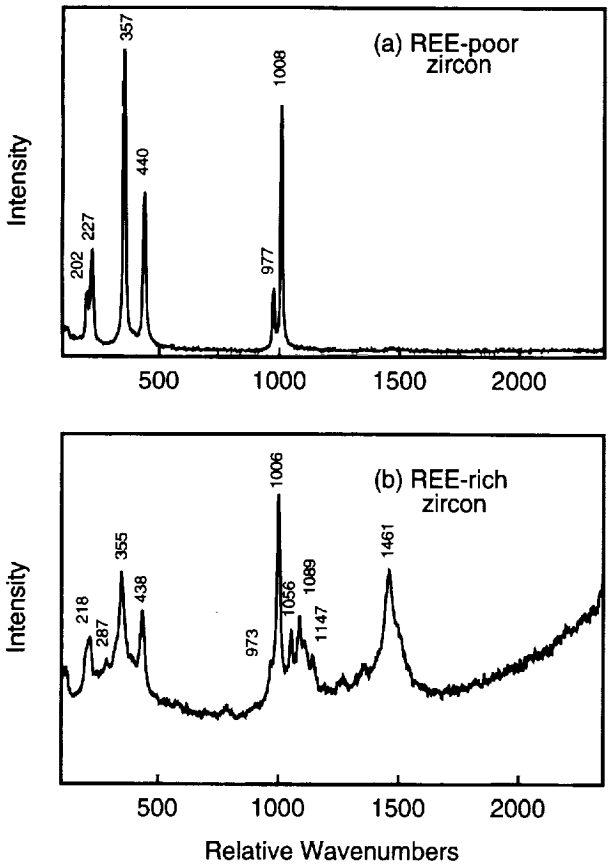

FIGURE 2. Examples of Raman spectra of (a) a trace element–poor and (b) a trace element–rich terrestrial zircon, obtained with an ISA S-3000 laser Raman microprobe and 514 nm excitation wavelength. The x axis is in units of relative wavenumbers (Δcm^{-1}) with respect to the excitation wavelength of 514 nm (19435 absolute cm^{-1}); y axis is in arbitrary intensity units. Peaks higher than 1008 Δcm^{-1} are the result of fluorescence caused by Er^{3+} and Eu^{3+}.

orescence, rather than by Raman scattering) may be observed (compare Figs. 2a and 2b).

Figure 3 shows the Raman spectra obtained from points A and E of the lunar zircon. Heavy trace element concentrations increase on the traverse from A to E and correlate with decreases in Raman band intensities, increases in Raman peak widths, and increases in background count rates. In addition, there is a shift in the peak position of the Si-O stretching mode and changes in the laser-in-

TABLE 2. Raman frequencies of zircon $ZrSiO_4$

ν_0 (Δ cm^{-1})	Symmetry	Assignment
1008	E_g	ν_3: SiO_4 antisymmetric stretch
974	A_{1g}	ν_1: SiO_4 symmetric stretch
439	A_{1g}	ν_2: SiO_4 antisymmetric bend
355	E_g	ν_4: SiO_4 symmetric bend
224	external mode	lattice mode, rotational
201	external mode	lattice mode, translational

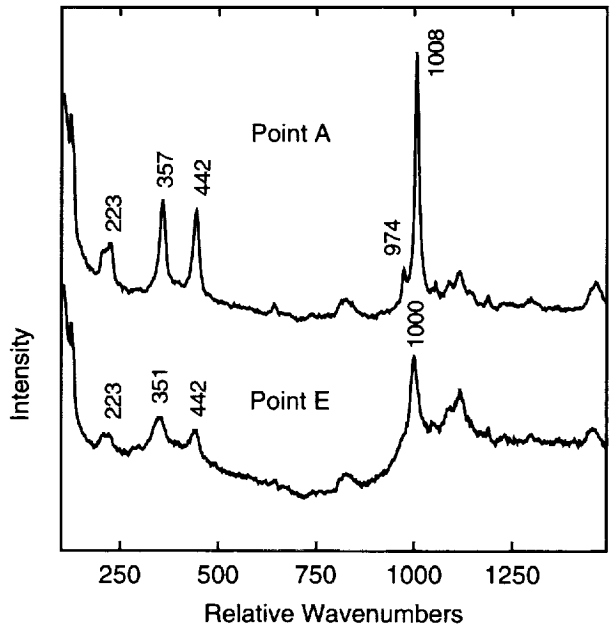

FIGURE 3. Raman spectra of sampling points A (trace element poor) and E (trace element rich) in zircon grain in lunar sample 14161,7069. The two spectra are plotted to the same scale but offset along the y axis with respect to each other.

duced fluorescence bands. The latter bands (which appear on the high-wavenumber side of the Si-O stretching vibrations in the case of excitation by the 514.5 nm wavelength) are more intense on the trace element–rich side of the grain (i.e., sampling point E). Figure 4 shows an expanded scale of the Si-O stretching region for all five sampling points. In a traverse from the trace element–poor side to the trace element–rich side of the grain, the following changes in the Si-O stretching mode are observed (from top to bottom in Fig. 4): The peak position changes from 1008 to 1000 Δcm^{-1}, the maximum intensity decreases from 1783 to 661 counts per second, the peak width at one-half height increases from 12.7 to 23.3 cm^{-1}, and the background increases from 390 to 728 counts per second.

RESULTS AND DISCUSSION

Chemical composition and zoning

The zircon grain is optically zoned across its long dimension in terms of its interference colors, with an estimated decrease in retardation of about 50%. From point A to point E (Fig. 1c), the observed color in transmitted, cross-polarized light changes from deep purple (~600 nm retardation) to light purple to yellow to white (first order, ~300 nm retardation) as the concentrations of U and Th increase from 21 to 55 ppm and 6 to 31 ppm, respectively. The concentrations of the REEs also increase from point A to point E (Table 1). In each of the five analysis points, the heavy REEs are strongly enriched relative to the light REEs (Fig. 5); this is typical for zircon and in

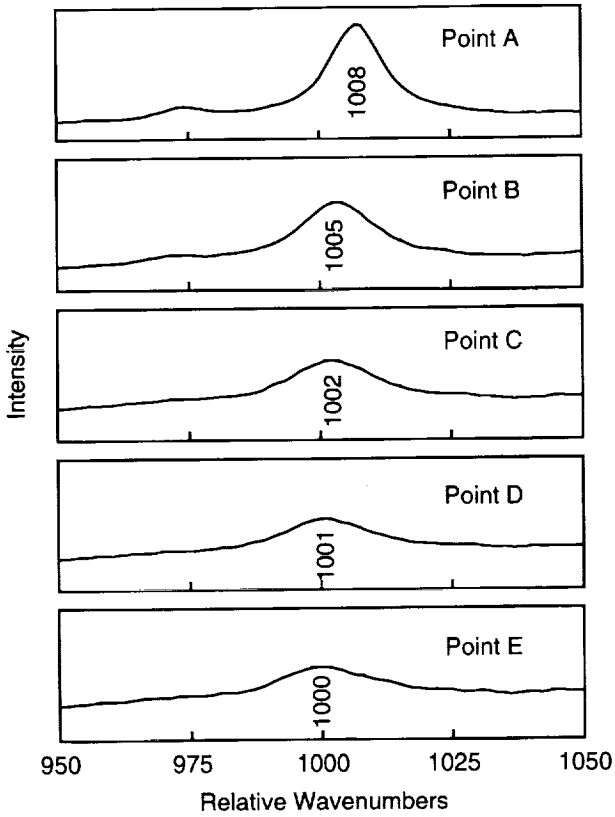

FIGURE 4. Enlargement of the Si-O stretching-mode peak from the Raman spectra, measured across a traverse (sampling points A through E; see Fig. 1) on the zircon grain in lunar sample 14161,7069. The *y* axes are in arbitrary-intensity units, but the same scale is used in all five spectra.

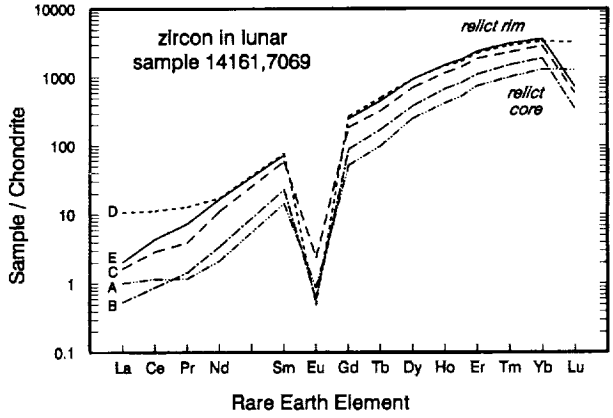

FIGURE 5. Chondrite-normalized REE concentrations as measured by SIMS analysis across a traverse (sampling points A through E; see Fig. 1) in the zircon grain in lunar sample 14161,7069. Although enigmatic, the anomalous decrease from Yb to Lu for spots B, C, and E does not appear to be an analytical artifact. Because the HREE concentrations are so high and the REE pattern rises sharply, the analysis of Lu is straightforward. Furthermore, more than a couple dozen analyses of terrestrial zircons, the Yb and Lu concentrations of which bracket those in the lunar zircon, show only a smooth increase from Yb to Lu.

accordance with the distribution coefficients for the REE between zircon and silicate melt, which are high for the heavy REEs but decrease strongly toward lighter REEs (e.g., Speer 1982; Hinton and Upton 1991).

The increase in mean atomic number across the zircon grain reflected in the backscattered electron image results from the progressive enrichment of heavy trace elements, principally the heavy REEs (Table 1; Fig 1b), not from substitution of Hf for Zr. In fact, the Zr/Hf ratio remains fairly constant across the grain, averaging ~48.9 (mass ratio) ± 2.7 (1σ standard deviation on the basis of ~60 electron microprobe spots). This is the same as the average Zr/Hf weight ratio given by Meyer et al. (1991) for many samples of lunar zircon.

The U and Th concentrations across the zircon grain are comparatively low for lunar zircon; U and Th concentrations in lunar zircon generally range from ~100 to 900 ppm and 50 to 1200 ppm, respectively (Compston et al. 1984; Hinton and Meyer 1991; Meyer et al. 1986, 1989b). The REE concentrations in the grain are also low for lunar zircon, using Y_2O_3, the geochemical behavior of which is similar to that of the HREEs, as a measure. Concentrations of Y_2O_3 in the zircon grain of this study range from 0.07 to 0.34 wt%, whereas Y_2O_3 concentrations range up to 1.6 wt%, with an average of 0.3–0.4 wt% in other samples of lunar zircon (Meyer et al. 1991).

Concentrations of the incompatible trace elements (ITEs) correlate strongly across the zircon grain (Fig. 6). In this context, the ITEs include those elements other than Zr and Hf that are typically incompatible in the major silicate minerals (Y, P, Ba, U, Th, and the trivalent lanthanides). We attribute the chemical zoning of the zircon grain to magmatic crystallization for reasons discussed below. We interpret the ITE-poor zone (Fig. 1c, point A) as a relict core, and the ITE-enriched zone (point E) as a relict rim. The dominant minerals throughout most of the crystallization interval of the original (precursor) igneous rock were pyroxene and plagioclase, which both strongly exclude ITEs, the concentrations of which increase in the zircon from point A to point E. Thus, the increase in concentrations of trace elements in the zircon may reflect a progressive enrichment of the ITEs in the residual melt from which the zircon crystallized.

Calculation of α-decay event dose

From radioactive decay of the ^{238}U, ^{235}U, and ^{232}Th isotopes, the number of α-decay events for the different U and Th concentrations may be calculated (Table 1). From the relationship $-dN/dt = \lambda N$, where N is the number of radioactive nuclei, λ is the decay constant, and dN is the number of decays in the interval dt, it follows that $N = N_0e^{-\lambda t}$, where N_0 is the number of radioactive nuclei at $t = 0$. Because the number of decay events for a given reaction is $N_0 - N$, the decay event dose for a single reaction is $D = N(e^{\lambda t} - 1)$. Using this relationship, we calculated the number of α decays for each of the three

series (Friedlander et al. 1981), the U series ($^{238}U \rightarrow {}^{206}Pb$), the actinium series ($^{235}U \rightarrow {}^{207}Pb$), and the Th series ($^{232}Th \rightarrow {}^{208}Pb$), assuming an age of 4.0 Ga. Because the half-lives of intermediate members of each series are short relative to the first transition in each series, we calculated the number of initial decays ($^{238}U \rightarrow {}^{234}Th$, $^{235}U \rightarrow {}^{231}Th$, $^{232}Th \rightarrow {}^{228}Ra$) and multiplied by the number of α decays in each series, 8, 7, and 6 for the U, actinium, and Th series, respectively (Holland and Gottfried 1955; Ellsworth et al. 1994). We assume that at present, ^{235}U makes up 0.72% and ^{238}U makes up 99.27% of the U that we measured with the ion microprobe.

For our sample, estimates calculated as described above are minimum values for two reasons. First, a small amount of the Th present may initially have been ^{244}Pu, which would have contributed three additional α-decay events per atom. However, the majority of α-decay events result from the U series (~68%) and actinium series (~26%), so any potential contribution from ^{244}Pu leading to ^{232}Th would be minor. Although the effective ionic radius of Pu^{4+} in eightfold coordination (0.96 Å) is very similar to that of U^{4+} (1.00 Å) (Shannon 1976), we know of no direct evidence for the incorporation of ^{244}Pu into ancient lunar zircon. The second reason that the α-decay event dose as calculated above is a minimum estimate is that, prior to thin-sectioning, this sample was irradiated with thermal neutrons for the purpose of instrumental neutron activation analysis (see Jolliff et al. 1991). We estimate, however, that nuclear reactions involving the actinides, resulting from neutron irradiation, produced $<10^{10}$ energetic decay events per milligram of zircon, including both α-decay and fission reactions. This is about four to five orders of magnitude less than that produced by the natural decay of U and Th isotopes over the ≥4 billion year lifetime of the grain (see below). Direct damage from fast neutrons may produce atomic displacements (Hobbs et al. 1994); however, this should have affected the zircon grain uniformly; thus, the variation in structural degradation from spot to spot as measured by the Raman microprobe was attributed to actinide-related α-decay events. In a typical neutron irradiation, <1% of each of the isotopes ^{238}U, ^{235}U, and ^{232}Th are converted to some other isotope.

On the basis of U and Th concentrations, the minimum dose of α-decay events is 5.2×10^{14} α decays per milligram of zircon (46 ppm U and 7 ppm Th, initially) in point A (i.e., the core) and 1.4×10^{15} α decays per milligram (122 ppm U and 38 ppm Th, initially) in point E (i.e., the rim). This is slightly less than the 2×10^{15} to 10^{16} events per milligram estimated by Chakoumakos et al. (1987) to be necessary for complete metamictization of zircon (see also Bursill and McLaren 1966; Woodhead et al. 1978; Murakami et al. 1991; Weber et al. 1994). On the basis of Raman spectral parameters that reflect structural degradation (as explained below), the process of structural degradation leading to metamictization began at a dose of $<10^{15}$ α-decay events per milligram of zircon.

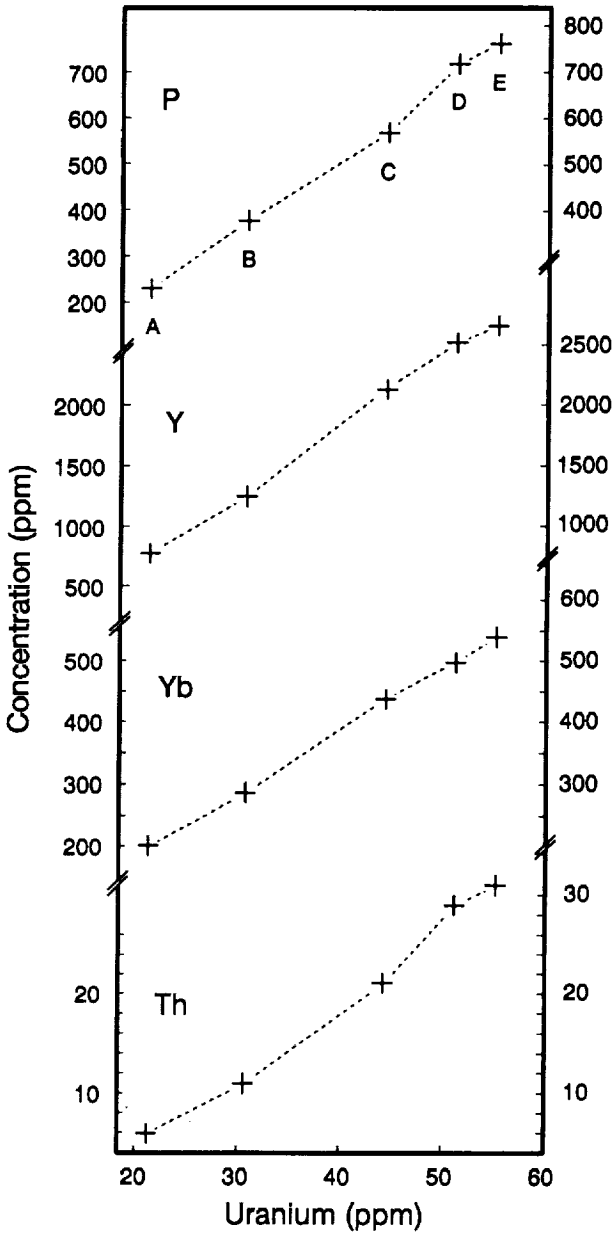

FIGURE 6. Correlation of the concentrations of U with concentrations of P, Yb, Y, and Th measured by SIMS analysis across the traverse (sampling points A through E; see Fig. 1) on the zircon grain in lunar sample 14161,7069. Size of plotting points equals or exceeds the analytical uncertainty (Table 2).

Raman parameters and their correlation to chemical zoning

Changes in the crystalline structure of zircon caused by the decay of U and Th have been previously described in the application of transmission electron microscopic and X-ray diffraction techniques (e.g., Bursill and McLaren 1966; Murakami et al. 1991). Nasdala et al. (1995) were the first to report the application of Raman spectroscopy to study this problem. Their data, and the data that we

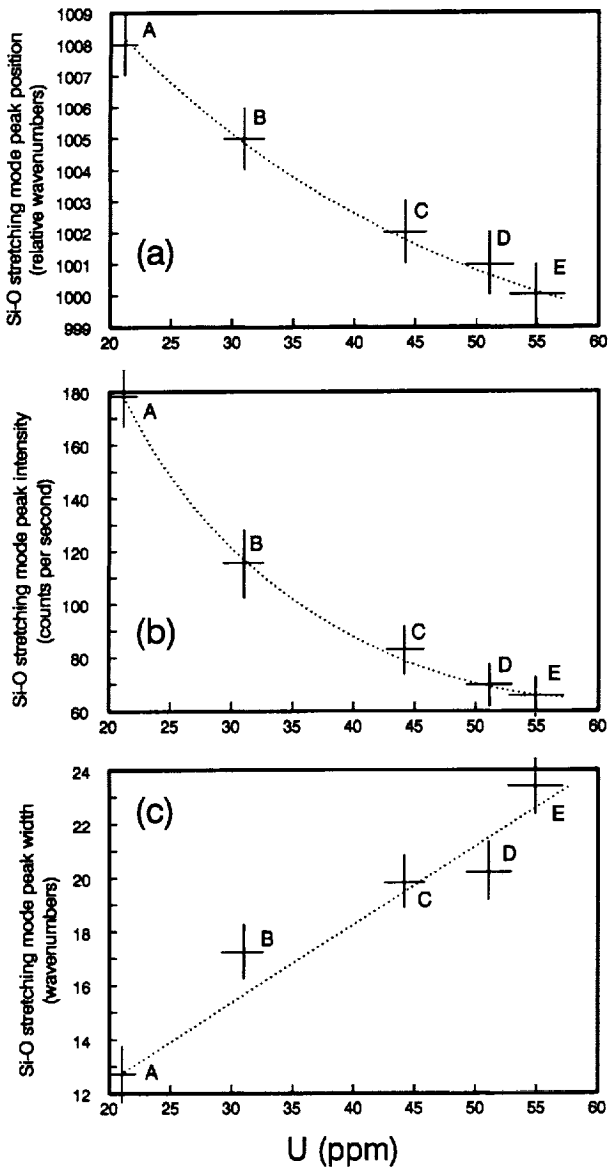

FIGURE 7. Concentration of U measured by SIMS vs. parameters obtained from the Raman spectra: (a) Si-O stretching-mode peak position; (b) Si-O stretching-mode peak intensity; (c) Si-O stretching-mode peak width. Analytical uncertainty is represented by the size of the symbols, except for c because the uncertainty in the peak width is unknown.

present here (abstracted in Jolliff et al. 1995), show that Raman spectroscopy is an effective method for measuring such changes in the crystalline structure of zircon. Raman parameters are sensitive to the structural degradation of the zircon lattice (Nasdala et al. 1995). The shift of Raman bands toward lower relative wavenumbers is attributed to an increase in interatomic distances, i.e., to a slight expansion of the lattice. The increase in band widths and the accompanying decrease of intensity are attributed to the fact that the distribution of bond lengths and bond angles within and between SiO_4 tetrahedra become increasingly irregular.

The observed variations in the Raman spectra correlate well with the variations in chemical composition of the lunar zircon grain as determined by electron microprobe and ion microprobe analyses. This crystal was the ideal sample to establish such a correlation because its orientation with respect to the laser beam remained unchanged during the Raman measurements across the crystal, thus eliminating crystal orientation as a factor in peak intensity variations.

Increasing concentrations from point A to point E of the heavy trace elements correlate with a continuous shift of the Si-O stretching mode from 1008 to 1000 Δcm^{-1} (Figs. 4 and 7a). In Figure 7a, this peak shift is plotted against the concentration of U, which gives the smoothest correlation. In agreement with Nasdala et al. (1995), we conclude that it is the structural damage from α-decay events that causes this peak shift. Also, the intensity of this Si-O stretching vibration correlates well with the U concentration (Fig. 7b): Areas of higher U concentration show less intense Raman peaks. In addition, there is a roughly linear correlation between the width of the Si-O stretching-mode peak and the U concentration (Fig. 7c): At higher U concentration, the band is wider. We attribute both of these phenomena, i.e., a decrease in peak intensity and an increase in peak width, to the transition from crystalline to structurally damaged zircon, i.e., to the increase in the degree of metamictization.

The optical and Raman spectral properties are consistent with an increased degree of metamictization across the grain. In general, broadening of Raman peaks may result from many physical phenomena such as small crystallite sizes [as is the case for disordered forms of graphite (Wopenka and Pasteris 1993)], the amorphous character of a sample (e.g., glasses are known to have very wide Raman peaks), or a high density of dislocations and point defects caused, for example, by α-particle damage (Murakami et al. 1991). The latter factor apparently is responsible for the wide Raman peaks observed in slightly metamict zircon.

An increased transmissivity to the 514 nm exciting laser light in sampling points D and E was observed. This is manifested in an increase in sensitivity to the heat of the laser beam by the mounting medium located underneath the zircon and may be caused by the structural degradation of the zircon in those sampling points. We previously found in our laboratory (unpublished results) that amorphous or disordered solids are more transmissive to the excitation wavelength of the laser than their crystalline equivalents. Partial or complete breakdown of zircon to baddelyite and silica glass has been reported from tektites and impact crater glasses (Kleinmann 1969). However, the Raman spectra of the metamict zones in the lunar zircon grain do not give any indication of the decomposition into SiO_2 and ZrO_2, both of which would

have distinct Raman spectra. This supports the interpretation that metamictization is a disorder phenomenon, the end product of which is a glassy state with zircon composition.

The laser-induced fluorescence observed in zircon is attributed to photoluminescence of trivalent REE ions that substitute for Zr^{4+} (e.g., Marfunin 1979). The fine structure of emission lines of the REE depends on the local crystal field around the REE ion and is thus unique to each host mineral. The only detailed study of laser-excited fluorescence of REE ions in a mineral (fluorite) was conducted by Burruss et al. (1992), who established a correlation between the REE concentration and the intensity of the fluorescence emission. All terrestrial and extraterrestrial samples of zircon that contain REE exhibit such laser-induced fluorescence emissions at specific wavelengths; those wavelengths are exactly the same for different zircon samples. A full analysis of these REE emission spectra will be reported in a subsequent paper. In this paper, we mention only that the 488 nm laser-excited fluorescence bands observed in zircon essentially define three groups: (1) from ~539 to ~558 nm, caused by Eu^{3+}, Er^{3+}, and Tb^{3+}, (2) from ~568 to ~582 nm, caused by Dy^{3+}, and (3) several more isolated bands at 604, 616, 650, and 660 nm, caused by Eu^{3+}. In comparison with bands of other samples of lunar and terrestrial zircon (unpublished data from our laboratory), the fluorescence bands in the zoned, single-crystalline zircon of this study are weak (even on the trace element–rich side of the crystal), consistent with the relatively low concentrations of REE in this sample. There is a strong linear correlation between the intensity of the emission line at 546 nm (caused by Er^{3+}) and the Er concentration as determined by ion microprobe analysis. The general applicability and usefulness of this finding needs testing, especially because the presence of crystalline disorder may complicate the quantitative interpretation of REE photoluminescence.

Quantification of the degree of structural disorder using Raman microprobe analysis may lead to a better understanding of the thermal history and the redistribution of radiogenic Pb, Th, U and other intermediate daughter products related to the expansion of the zircon structure owing to metamictization. Further studies of zircon need to address the following questions: (1) Can the observed variations in the Raman spectra of zircon be calibrated against the U concentration or the sum of heavy trace elements present in any given sample? (2) Can the interpretation of Raman spectra provide a general means of quantifying the degree of metamictization? (3) Can the Raman microprobe be used to quantify and evaluate the degree of self-annealing over extended geologic time, as suggested to occur by Weber et al. 1994? (4) Is there a generally applicable correlation between REE concentrations and the intensity of the laser-induced fluorescence emissions? (5) Does the strong correlation between Raman parameters and trace element concentrations in the lunar zircon also hold for zircon that has been subjected to terrestrial igneous and metamorphic processes?

Acknowledgments

We are grateful to Trevor Ireland for providing a series of zircon standards with known Th and U concentrations. We also thank Conel Alexander for his help with ion microprobe data analysis. We thank Rodney Ewing and Richard Hinton for their thorough and very helpful reviews of the manuscript. Partial funding for this work was provided by NASA grant NAGW-3343 (to B.L.J.), NSF grant GER-9023520 (to B.W.), NSF grant EAR-9417677 (to B.W.), and NASA grant NAGW-3371 (to E.Z.).

References cited

Armstrong, J.T. (1988) Quantitative analysis of silicate and oxide minerals: Comparison of Monte-Carlo, ZAF, and phi-rho-Z procedures. Microbeam Analysis, 239–246.

Black, L.P., Kinny, P.D., and Sheraton, J.W. (1991) The difficulties of dating mafic dykes: An Antarctic example. Contributions to Mineralogy and Petrology, 109, 183–194.

Burruss, R.C., Ging, T.G., Eppinger, R.G., and Samson, I.M. (1992) Laser-excited fluorescence of rare earth elements in fluorite: Initial observations with a laser Raman microprobe. Geochimica et Cosmochimica Acta, 56, 2713–2723.

Bursill, L.A., and McLaren, A.C. (1966) Transmission electron microscope study of natural radiation damage in zircon ($ZrSiO_4$). Physica Status Solidi, 13, 331–343.

Chakoumakos, B.C., Murakami, T., Lumpkin, G.R., and Ewing, R.C. (1987) Alpha-decay-induced fracturing in zircon: The transition from crystalline to the metamict state. Science, 236, 1556–1559.

Compston, W., Williams, I.S., and Meyer, C. (1984) U-Pb geochronology of zircons from lunar breccia 73217 using a sensitive high mass-resolution ion microprobe. Proceedings of the 14th Lunar and Planetary Science Conference, in Journal of Geophysical Research, 89, B525–B534.

——— (1989) The problem of lunar initial Pb. Lunar and Planetary Science, XX, 179–180.

Crozaz, G., and Zinner, E. (1986) Quantitative ion microprobe analysis of the rare earth elements in minerals. Scanning Electron Microscopy, II, 369–376.

Dawson, P., Hargreave, M.M., and Wilkinson, G.R. (1971) The vibrational spectrum of zircon ($ZrSiO_4$). Journal of Physics: Solid State Physics, 4, 240–256.

Ellsworth, S., Navrotsky, A., and Ewing, R.C. (1994) Energetics of radiation damage in natural zircon ($ZrSiO_4$). Physics and Chemistry of Minerals, 21, 140–149.

Ewing, R.C., Lutze, W., and Weber, W.J. (1995) Zircon: A host-phase for the disposal of weapons plutonium. Journal of Materials Research, 10, 243–246.

Friedlander, G., Kennedy, J.W., Macias, E.S., and Miller, J.M. (1981) Nuclear and radiochemistry (3rd edition), 684 p. Wiley, New York.

Hinton, R.W., and Meyer, C. (1991) Ion microprobe analysis of zircon and yttrobetafite from a lunar granite. Lunar and Planetary Science, XXII, 575–576.

Hinton, R.W., and Upton, B.G.J. (1991) The chemistry of zircon: Variations within and between large crystals from syenite and alkali basalt xenolyths. Geochimica et Cosmochimica Acta, 55, 3287–3302.

Hobbs, L.W., Clinard, F.W., Zinkle, S.J., and Ewing, R.C. (1994) Radiation effects in ceramics. Journal of Nuclear Materials, 216, 291–321.

Holland, H.D., and Gottfried, D. (1955) The effect of nuclear radiation on the structure of zircon. Acta Crystallographica, 8, 291–300.

Ireland, T.R., Fahey, A.J., and Zinner, E.K. (1991) Hibonite-bearing microspherules: A new type of refractory inclusions with large isotopic anomalies. Geochimica et Cosmochimica Acta, 55, 367–379.

Jarosevich, E., and Boatner, L.A. (1991) Rare-earth element reference samples for electron microprobe analysis. Geostandard Newsletter, 15, 397–399.

Jolliff, B.L. (1991) Fragments of quartz monzodiorite and felsite in Apollo

14 soil particles. Proceedings of Lunar and Planetary Science, 21, 101–118.

Jolliff, B.L., Korotev, R.L., and Haskin, L.A. (1991) Geochemistry of 2–4 mm particles from Apollo 14 soil (14161) and implications regarding igneous components and soil-forming processes. Proceedings of Lunar and Planetary Science, 21, 193–219.

Jolliff, B.L., Wopenka, B., Zinner, E., and Kremser, D.T. (1995) A zoned lunar zircon in a quartz-monzodiorite breccia from Apollo 14: U, Th, other trace elements, and Raman spectral parameters. Lunar and Planetary Science, XXVI, 695–696.

Kleinmann, B. (1969) The breakdown of zircon observed in the Libyan desert glass as evidence of its impact origin. Earth and Planetary Science Letters, 5, 497–501.

Marfunin, A.S. (1979) Spectroscopy, luminescence and radiation centers in minerals, 352 p. Springer-Verlag, New York.

McLaren, A.C., FitzGerald, J.D., and Williams, I.S. (1994) The microstructure of zircon and its influence on the age determination from Pb/U isotopic ratios measured by ion microprobe. Geochimica et Cosmochimica Acta, 58, 993–1005.

Meyer, C., Williams, I.S., and Compston, W. (1986) Direct evidence of ancient lunar granite. In 6th International Conference on Geochronology and Isotope Geology, Terra Cognita, 6, 173.

Meyer, C., and Yang, S.V. (1988) Tungsten-bearing yttrobetafite in lunar granophyre. American Mineralogist, 73, 1420–1425.

Meyer, C., Williams, I.S., and Compston, W. (1989a) $^{207}Pb/^{206}Pb$ ages of zircon-containing rock fragments indicate continuous magmatism in the lunar crust from 4350 to 3900 million years. Lunar and Planetary Science, XX, 691–692.

——— (1989b) Zircon-containing rock fragments within Apollo 14 breccia indicate serial magmatism from 4350 to 4000 million years. In G.J. Taylor and P.H. Warren, Eds., Workshop on Moon in transition: Apollo 14, KREEP, and evolved lunar rocks, p. 75–78. Lunar and Planetary Institute Technical Report 89–03, Lunar and Planetary Institute, Houston, Texas.

Meyer, C., Galindo, C., and Yang, S.V. (1991) Lunar zircon. Lunar and Planetary Science, XXII, 895–896.

Murakami, T., Chakoumakos, B.C., Ewing, R.C., Lumpkin, G.R., and Weber, W.J. (1991) Alpha-decay event damage in zircon. American Mineralogist, 76, 1510–1532.

Nasdala, L., Irmer, G., and Wolf, D. (1995) The degree of metamictization in zircon: A Raman spectroscopic study. European Journal of Mineralogy, 7, 471–478.

Pidgeon, R.T. (1992) Recrystallization of oscillatory zoned zircon: Some geochronological and petrological implications. Contributions to Mineralogy and Petrology, 110, 463–472.

Pidgeon, R.T., O'Neill, J.R., and Silver, L.T. (1966) Uranium and lead isotopic stability in a metamict zircon under experimental conditions. Science, 154, 1538–1540.

Sahama, T.G. (1981) Growth structure in Ceylon zircon. Bulletin de Mineralogie, 104, 89–94.

Shannon, R.D. (1976) Revised effective ionic radii and systematic studies of interatomic distances in halides and chalcogenides. Acta Crystallographica, A32, 751–767.

Shih, C.-Y., Nyquist, L.E., Bogard, D.D., Wooden, J.L., Bansal, B.M., and Wiesmann, H. (1985) Chronology and petrogenesis of a 1.8 g lunar granitic clast: 14321,1062. Geochimica et Cosmochimica Acta, 49, 411–426.

Shih, C.-Y., Nyquist, L.E., and Wiesmann, H. (1993) K-Ca chronology of lunar granites. Geochimica et Cosmochimica Acta, 57, 4827–4841.

Silver, L.T., and Deutsch, S. (1963) Uranium-lead isotopic variations in zircons: A case study. Journal of Geology, 71, 721–729.

Smith, J.V., and Steele, I.M. (1976) Lunar mineralogy: A heavenly detective story, Part II. American Mineralogist, 61, 1059–1116.

Speer, J.A. (1982) Zircon. In American Mineralogical Society Reviews in Mineralogy, 5, 67–112.

Tilton, G.R. (1960) Volume diffusion as a mechanism for discordant lead ages. Journal of Geophysical Research, 65, 2933–2945.

Wark, D.A., Reid, A.F., Lovering, J.F., and El Goresy, A. (1973) Zirconolite (versus zirkelite) in lunar rocks. Lunar Science, IV, 764–766.

Warren, P.H. (1989) KREEP: Major-element diversity, trace-element uniformity (almost). In G.J. Taylor and P.H. Warren, Eds., Workshop on Moon in transition: Apollo 14, KREEP, and evolved lunar rocks, p. 149–153. Lunar and Planetary Institute Technical Report 89–03, Lunar and Planetary Institute, Houston, Texas.

——— (1993) A concise compilation of petrologic information on possibly pristine nonmare Moon rocks. American Mineralogist, 78, 360–376.

Weber, W.J., Ewing, R.C., and Wang, L.M. (1994) The radiation-induced crystalline-to-amorphous transition in zircon. Journal of Materials Research, 9, 688–698.

Williams, I.S., Compston, W., Black, L.P., Ireland, T.R., and Foster, J.J. (1984) Unsupported radiogenic Pb in zircon: A cause of anomalously high Pb-Pb, U-Pb and Th-Pb ages. Contributions to Mineralogy and Petrology, 88, 322–327.

Woodhead, J.A., Rossman, G.R., and Silver, L.T. (1978) X-ray and infrared studies of zircon metamictization. Eos, 59, 394.

——— (1991) The metamictization of zircon: Radiation dose-dependent structural characteristics. American Mineralogist, 76, 74–82.

Wopenka, B., and Pasteris, J.D. (1993) Structural characterization of kerogens to granulite-facies graphite: Applicability of Raman microprobe spectroscopy. American Mineralogist, 78, 533–557.

Yada, K., Tanji, T., and Sunagawa, I. (1981) Application of lattice imagery to radiation damage investigation in natural zircon. Physics and Chemistry of Minerals, 7, 47–52.

Zinner, E., and Crozaz, G. (1986) A method for the quantitative measurement of rare earth elements in the ion microprobe. International Journal for Mass Spectrometry and Ion Processes, 69, 17–38.

MANUSCRIPT RECEIVED JULY 2, 1995
MANUSCRIPT ACCEPTED MARCH 26, 1996